Indian Ocean Dipole intensifies Benguela Niño through Congo River discharge

Check for updates

Michael J. McPhaden [1] ✉, Sreelekha Jarugula[2], Léo C. Aroucha [3] & Joke F. Lübbecke [3]

Benguela Niños are episodes of unusual El Niño-like warming in the upwelling zone off the coast of southwest Africa, with consequential impacts on marine ecosystems, coastal fisheries and regional weather. The strongest Benguela Niño in the past 40 years occurred in February–April 1995 with local sea surface temperature anomalies up to 4 °C off the coast of Angola and Namibia. Here, we show that a strong Indian Ocean Dipole in September–November 1994 helped boost the amplitude of the 1995 Benguela Niño through a land bridge involving Congo River discharge. We use atmospheric, oceanic, and hydrological data to demonstrate the sequential linkage between Indian Ocean Dipole development, unusually high rainfall in the Congo River basin, high Congo River discharge, low salinity near the Congo River mouth, and southward advection of this low salinity water into the Benguela upwelling region. The low salinity water isolated the surface mixed layer from the thermocline, which limited vertical mixing with colder subsurface waters and led to enhanced sea surface temperature warming. We also discuss how other Indian Ocean Dipole events may have similarly affected subsequent Benguela Niños and the possibility that Indian Ocean Dipole impacts on Benguela Niños may become more prominent in the future.

Benguela Niños are episodes of unusual warming that develop every few years in the upwelling zone off the coast of southwest Africa with consequential impacts on regional marine ecosystems, coastal fisheries and weather variability[1–4]. These events typically occur in late boreal winter-early spring (February–April) and are generated through wind-forced dynamical processes originating in the Atlantic basin involving either a weakening of the trade winds along the equator[5–7], a local weakening of the alongshore winds off of west Africa[8,9], or a combination of the two[10,11]. The strongest Benguela Niño in the past 40 years occurred in February–April 1995[12,13], with temperature anomalies in early 1995 reaching 2 °C above normal on average off the coast of Angola and Namibia and up to 4 °C in localized areas (Fig. 1a, d). This extreme warming was associated with increased mortality and southward migration of fish stocks such as sardines, horse mackerel, and kob off the coast of Angola[12].

While dynamical processes internal to the Atlantic basin generate Benguela Niños, it has recently been argued that the extraordinary warming in early 1995 was boosted by southward advection of unusually high freshwater discharge from the Congo River and precipitation over the western African coast[13]. Anomalous alongshore flow advected Congo River discharge southward to the Benguela upwelling region where it led to the formation of shallow freshwater mixed layers above thick salt-stratified barrier layers that limited vertical turbulent mixing with colder

thermocline waters below. The reduction in vertical mixing then caused SSTs to sharply rise in the surface mixed layer[13].

Why the Congo River discharge was high in early 1995 is an open question. Here, we will identify the cause of that high discharge as an Indian Ocean Dipole (IOD) event, one of the strongest of the past 40 years, that occurred in late 1994 (Fig. 1b, c). The IOD[14,15], which is similar to the Pacific El Niño that develops every few years through coupled ocean-atmosphere interactions involving surface wind and sea surface temperature (SST) variations, is a major source of year-to-year variability in Congo River basin rainfall[16,17] and Congo River discharge[17]. It has further been shown, by highlighting two recent extreme IOD events of opposite sign in 2016 and 2019 and by analyzing historical data over the last 40–60 years, that there is a direct link between the IOD, Congo River rainfall, Congo River discharge, and eastern tropical Atlantic sea surface salinity (SSS)[17]. There is a delay of several months between the peak of an IOD event, which typically occurs in boreal fall (September–November), and the peak eastern tropical Atlantic SSS anomaly because of intrinsic lags between changes in Indian Ocean SSTs, changes in atmospheric circulation and rainfall, Congo river basin hydrology, and river discharge.

We will demonstrate that linkages previously described[17], involving oceanic, atmospheric, and hydrological processes connecting the Indian and Atlantic Oceans, were clearly at work in late 1994 to early 1995. We will also

[1]NOAA Pacific Marine Environmental Laboratory, Seattle, WA, USA. [2]Jet Propulsion Laboratory, California Institute of Technology, Pasadena, CA, USA. [3]GEOMAR Helmholtz Centre for Ocean Research Kiel, Kiel, Germany. ✉e-mail: michael.j.mcphaden@noaa.gov
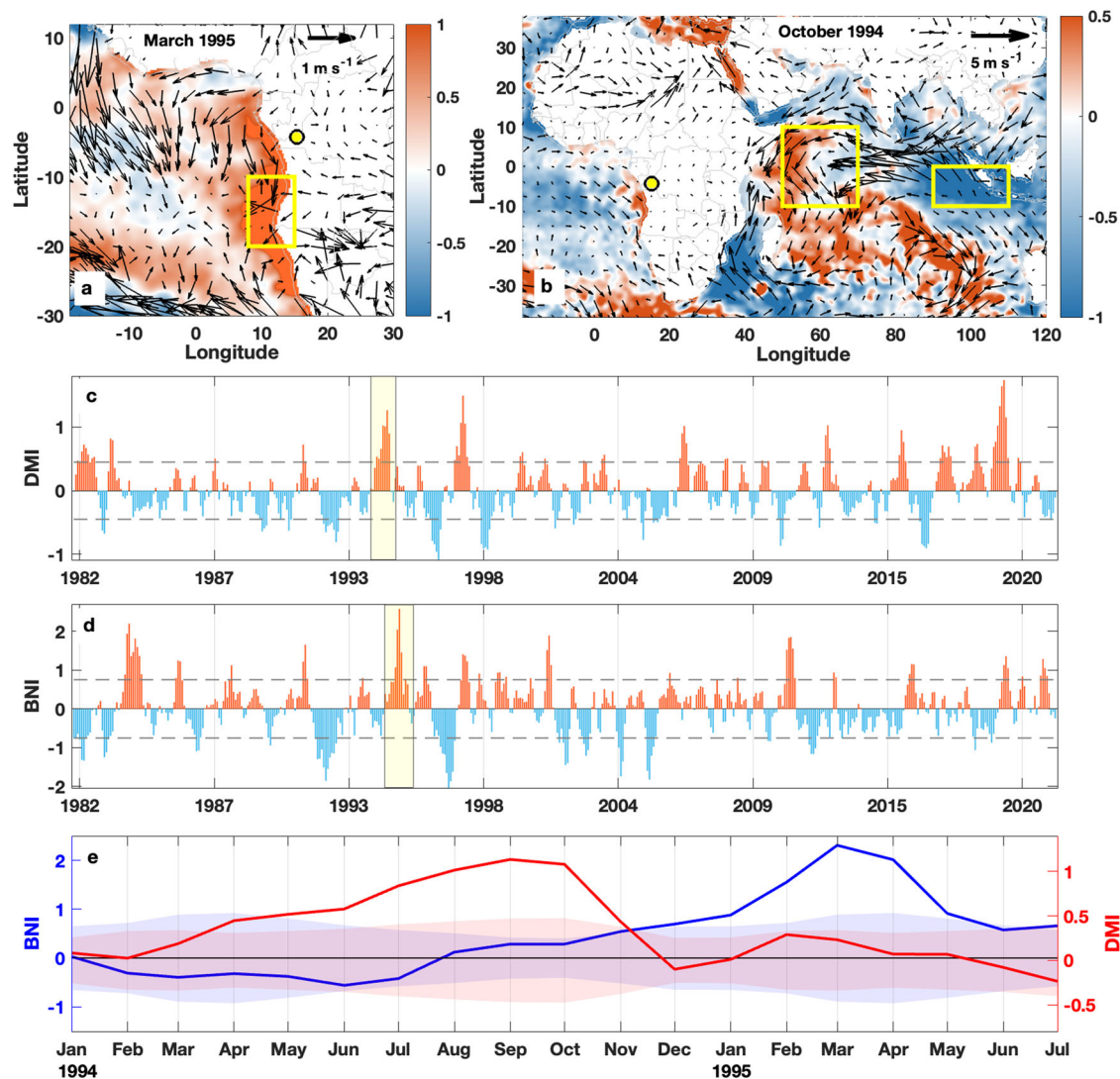
Fig. 1 | Indian Ocean Dipole and Benguela Niño Indices. Monthly sea surface temperature (SST) anomaly (shading, °C) in (**a**) March 1995 and (**b**) October 1994 relative to a monthly climatology for 1991–2020. Wind anomalies from the European Centre for Medium-Range Weather Forecasts Reanalysis v5 (ERA5) relative to a 1987–2020 climatology (vectors, in m s⁻¹) are overplotted. **c** Monthly Dipole Mode Index (DMI, °C) and (**d**) Benguela Nino Index (BNI, °C) estimated from SST for 1982–2021 with the 1994 and 1995 events outlined in yellow shading. Horizontal dashed lines are drawn for ±1 standard deviation which is often used as a threshold for defining significant events. **e** The DMI and BNI during January 1994–June 1995 with ±1 monthly standard deviation (shaded area) computed based on the period 1991–2020. The monthly time series in (**e**) are slightly smoothed with a 1–2–1 digital filter for clarity. BNI is calculated as the SST anomaly over the Angola-Benguela Area (10°S–20°S, 8°E–14°E; yellow box in **a**). The DMI is calculated as the SST anomaly difference between the eastern (10°S–0°N, 90°E–110°E) and western (10°S–10°N, 50°E–70°E) equatorial Indian Ocean (yellow boxes in **b**).

show that the resultant eastern tropical Atlantic SSS anomalies that were generated in early 1995 by the 1994 IOD event are the same as those identified as having intensified the 1995 Benguela Niño[13]. Finally, we will argue that the IOD may have been a factor in amplifying other Benguela Niño events through its impacts on eastern tropical Atlantic salinity such as in early 2016[9], a moderate amplitude Benguela Niño that was preceded by a moderate IOD event in late 2015[18].

Results and discussion
Development of the 1994 Indian Ocean Dipole
As is typical of most IOD events, the 1994 IOD began to develop in boreal spring, peaked in September to November, and then rapidly decayed by early 1995 (Fig. 1). During the peak phase in October 1994, rainfall was anomalously high in the Congo River basin (Fig. 2a, b) with a broad consistency in the spatial structure of rainfall within the basin exhibited by two different rainfall products (Fig. 2e, f). This rainfall was associated with a low-level wind convergence mainly driven by strong easterly wind anomalies from the

western Indian Ocean (Fig. 3). We can quantify the relationship of the large-scale wind field to Congo River basin rainfall through an analysis of the column integrated moisture budget (see "Data and Methods"), which indicates that the excess of precipitation over evaporation in the Congo River basin in October 1994 was the result of moisture convergence into the region with little contribution from changes in the column integrated moisture content (Fig. 4a–c). Moreover, focusing on October, which is typically in the peak season of IOD development, a decomposition of the moisture balance into contributions related to dynamic changes in atmosphere circulation vs thermodynamic contributions related to changes in atmospheric humidity (see "Data and Methods") indicates that in general it is predominantly changes in atmospheric circulation that control the moisture convergence and rainfall in the Congo River basin rather than changes in humidity (Fig. 4d).

Effects on Congo River discharge and coastal zone salinity
Congo River discharge measured at the Kinshasa-Brazzaville station, about 500 km upstream of the river mouth, provides an estimate of the outflow for
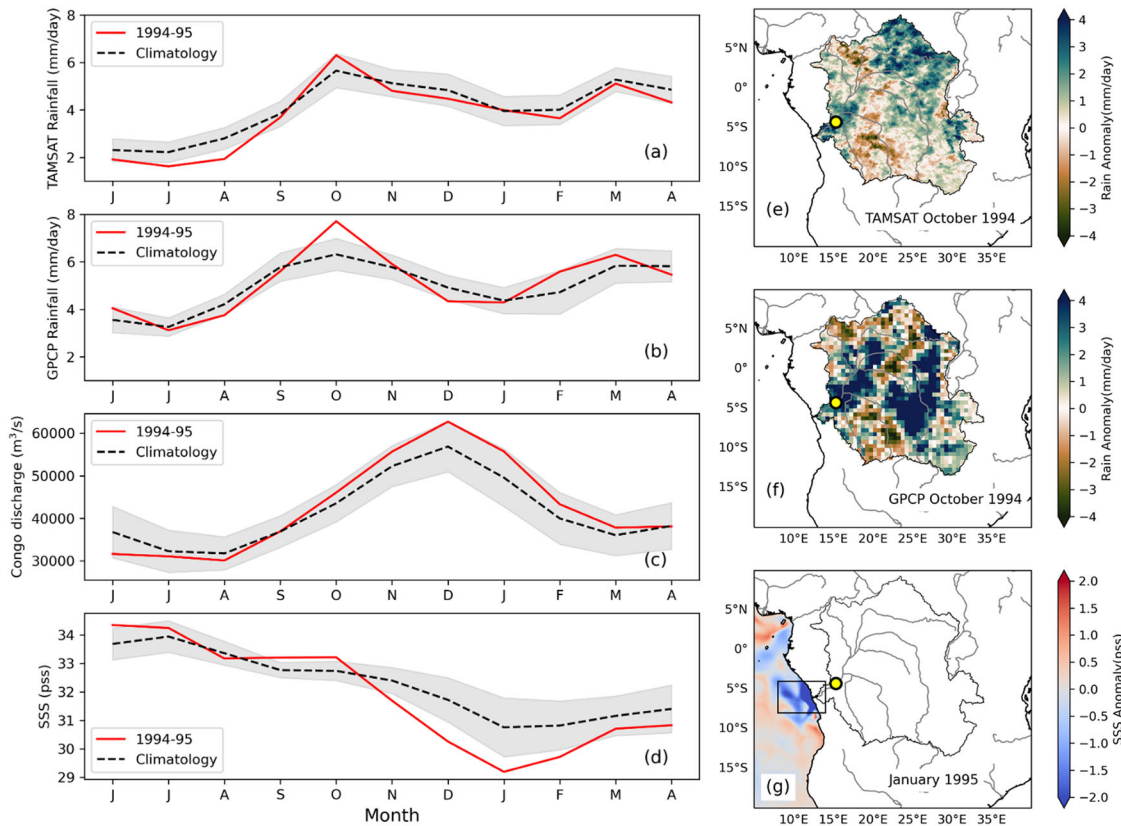
Fig. 2 | Congo basin rainfall, Congo River discharge, and sea surface salinity near the Congo River mouth from July 1994 to April 1995. Monthly mean values of (**a**) Tropical Applications of Meteorology using SATellite (TAMSAT) rainfall (mm day⁻¹) and (**b**) Global Precipitation Climatology Project (GPCP) rainfall (mm day⁻¹) averaged over the Congo basin, **c** Congo River discharge (m³ s⁻¹) measured at the Kinshasa-Brazzaville station (yellow dot in **e**–**g**) and (**d**) Global Ocean Eddy-resolving Reanalysis (GLORYS12) sea surface salinity (SSS; pss) averaged over coastal ocean near the Congo River mouth (4°S–8°S, 8°E–14°E; black box marked in

g) during June 1994 to March 1995 (red lines). Monthly climatologies (black dotted lines) and ±1 standard deviation (gray shading) are shown in (**a**–**d**). Spatial distribution of monthly rainfall anomalies (mm day⁻¹) over Congo basin in October 1994 from (**e**) TAMSAT and (**f**) GPCP. **g** Spatial map of monthly GLORYS12 reanalysis SSS anomaly (pss) in January 1995. The anomalies are estimated using monthly climatology during the period 1983–2020 for TAMSAT and GPCP rainfall, 1950–2019 for Congo River discharge and 1994–2020 for reanalysis SSS.
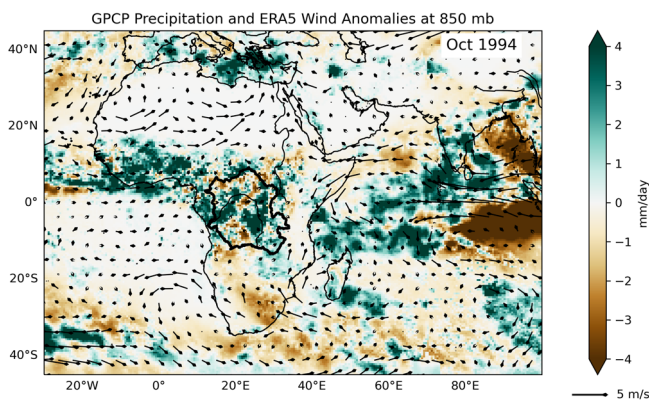
Fig. 3 | Anomalous low-level winds and rainfall around Africa in October 1994. Global Precipitation Climatology Project (GPCP) precipitation anomalies (shading, mm day⁻¹) are overplotted on 850 mb wind anomalies relative to a 1987–2020 climatology (vectors, in ms⁻¹) based on the European Centre for Medium-Range Weather Forecasts Reanalysis v5 (ERA5).

over 98% of the Congo River Basin[19]. Peak Congo River discharge occurs typically during December–January and was significantly higher than normal during November 1994 to January 1995 (by ~1 standard deviation) following the peak IOD and associated Congo basin rainfall anomaly (Fig. 2c). The delay of a few months from the peak Dipole Mode Index

(DMI) results from the time it takes for the atmospheric circulation to adjust to coupled ocean-atmosphere interactions in the Indian Ocean, for the circulation to converge the moisture over the Congo basin, and for the tributaries of the Congo River to funnel the runoff to the river mouth[17].

SSS began to drop in the coastal zone of the eastern tropical Atlantic as the anomalously large volume of Congo River water was discharged into the eastern Atlantic (Figs. 2c, d and 5). SSS anomalies lag Congo River discharge anomalies by about 1 month (Fig. 5) and the peak DMI by 3–5 months (Fig. S1), consistent with previous analysis[17]. Thus, the largest SSS anomalies near the mouth of the Congo occurred from December 1994 to February 1995 (Figs. 2d, g and 6b, c). There was a small contribution of local fresh-water forcing to the accumulation of low salinity water near the Congo River mouth in November and December 1994 (Fig. 5) because this is the time of year when the Intertropical Convergence Zone is shifted to the south of the equator in the eastern tropical Atlantic[19]. However, that contribution, even though enhanced relative to normal years (Fig. 5), was small relative to Congo River discharge.

Impact of fresh water on 1995 Benguela Niño development
The anomalous surface freshwater pool near the Congo River mouth was very thin, only 5–15 m deep[13]. Once established in January 1995, the freshwater pool was advected southward to the Angola-Benguela Area (ABA, defined as 10°–20°S, 8°E–14°E) by very strong surface southward flows near the African coast most notably in February 1995 (Fig. 6c, e). This anomalous southward flow resulted from a downwelling coastal Kelvin-wave remotely forced by weakening of the easterly trade winds near the
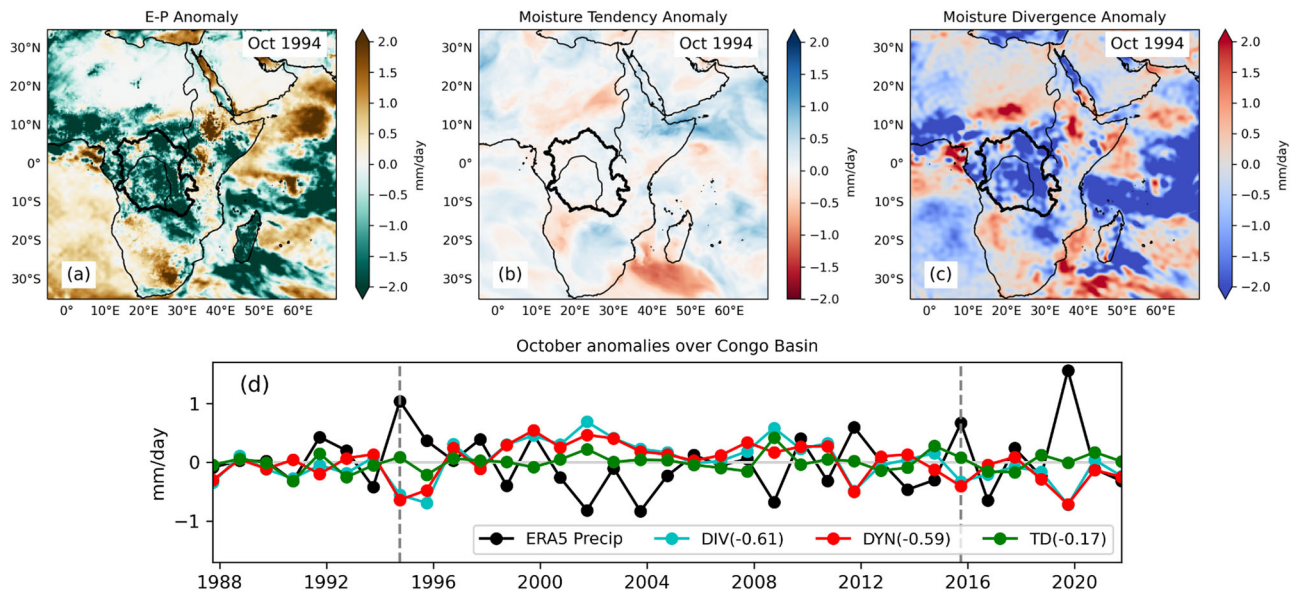
Fig. 4 | Atmospheric moisture budget anomalies for the Congo River basin.
October 1994 anomalies relative to a 1987–2020 climatology for (**a**) Evaporation minus precipitation ($E - P$), **b** column integrated moisture time tendency ($\partial q/\partial t$) and (**c**) moisture divergence flux ($\nabla.(qV)$) based on the European Centre for Medium-Range Weather Forecasts Reanalysis v5 (ERA5). The Congo River basin is outlined in each panel. **d** Detrended monthly anomalies for October precipitation (black), moisture divergence (DIV; blue), and dynamic (DYN; red) and thermo-dynamic (TD; green) components of moisture divergence averaged over the Congo basin based on the ERA5 reanalysis, with October 1994 and October 2015 marked by a dashed line. Correlation coefficients between DIV, DYN, TD, and the corresponding precipitation anomaly are indicated in parentheses. Standard deviations of DIV, DYN, and TD for October 1987–2020 are 0.33, 0.30, and 0.14, respectively. The correlations and standard deviations indicate the dominance of year-to-year variations in atmospheric circulation in determining the moisture divergence and rainfall over the Congo basin. All units in mm day^{-1}.
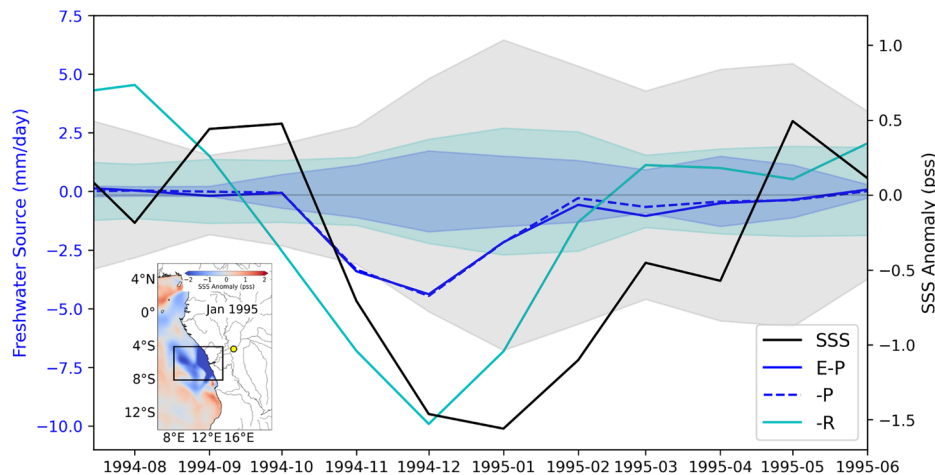

Fig. 5 | Congo River discharge is the dominant source of freshwater in the area surrounding the Congo River mouth in late 1994-early 1995. Monthly anomaly time series of sea surface salinity (SSS), evaporation minus precipitation ($E - P$) and river discharge per unit area ($-R$, with the negative sign to indicate a freshening effect on SSS) near the mouth of the Congo River (the oceanic area within 4°S–8°S, 8°E–14°E highlighted in the lower left inset) for July 1994–June 1995. $E - P$ based on the European Centre for Medium-Range Weather Forecasts Reanalysis v5 (ERA5) and SSS is from the Global Ocean Eddy-resolving Reanalysis (GLORYS12). For reference, $-P$ (which dominates $E - P$) is also plotted. Anomalies are computed relative to a 1994–2020 climatology with ±1 standard deviation for each term (shading) estimated from these anomalies. The standard deviation for $-P$ is not shown for clarity; it is nearly equivalent to the standard deviation of $E - P$. Consistent with ref. 13, Congo River discharge is larger in magnitude than $E - P$ and $-P$ in the vicinity of the Congo River mouth in late 1994-early 1995 and primarily responsible for the observed drop in SSS at that time.

equator[10] reinforced by a weakening of the alongshore local winds that also favored anomalous southward flow[13,20]. Some freshwater was advected offshore via eddies generated by the plume itself[21,22] (Fig. 6d) but the bulk remained trapped to the coast of Angola and Namibia resulting in thin (5–15 m deep) surface mixed layers resting above thick salt-stratified barrier layers (Fig. 7)[13]. These barrier layers were thickest in March–April 1995 coincident with the highest SSTs during the event. The strong shallow vertical density stratification due to low surface salinities limited vertical turbulent mixing with colder thermocline water below, which amplified warm mixed-layer temperature anomalies as shown in the surface layer temperature balance analysis conducted by ref. 13. Local precipitation contributed to some surface freshening in the ABA particularly in March 1995 as coastal SSTs reached their peak, resulting in anomalous deep convection and rainfall over the warm SSTs (Fig. 6e)[13]. Overall however, the largest source of freshening in the ABA in early 1995 was by far southward advection of Congo River discharge (Fig. 5).
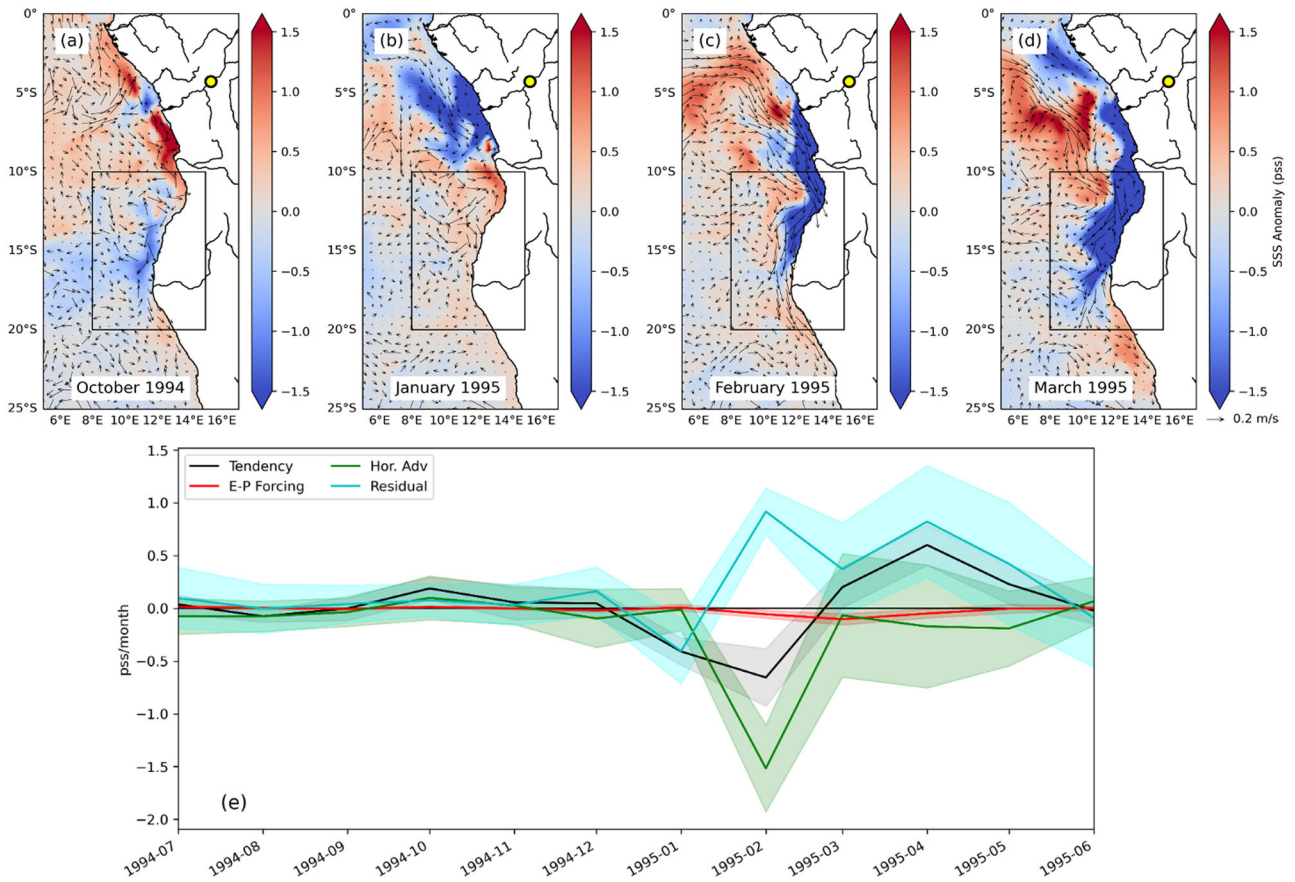
Fig. 6 | Surface salinity, surface currents, and mixed-layer salt balance in the eastern tropical Atlantic in late 1994-early 1995. Spatial maps of monthly Global Ocean Eddy-resolving Reanalysis (GLORYS12) SSS anomaly (pss; color) overlaid by surface velocity vector anomalies during (**a**) October 1994 (**b**) January 1995 (**c**) February 1995 and (**d**) March 1995 off the southwest coast of Africa. The Angola-Benguela Area (ABA; 10°S–20°S, 8°E–14°E) is indicated by the black box. Monthly anomalies are constructed relative to a 1994–2020 climatology. A reference vector of 0.2 m s^{-1} is shown in the bottom right. **e** Salt balance averaged over the ABA based on Eq. (1) in "Data and Methods", showing the time tendency for SSS anomalies (black curve), the anomalous local freshwater forcing term related to evaporation minus precipitation ($E − P$, red curve) and horizontal advection (green curve). Also shown is the residual (light blue curve) which includes terms that cannot be explicitly computed, such as vertical advection, entrainment, and diffusion, plus any computational errors. The ±1 standard deviation for each term (shading) is computed from monthly anomalies over the period 1994–2020. The large negative value of advection in February 1995 is mostly due to freshwater advection from the north. The large positive residual in February–April 1995 is consistent with an upward flux of high salinity water across the base of the salt-stratified mixed layer due to turbulent vertical mixing. Since there is no vertical temperature gradient at the base of the mixed layer (Fig. 7) this vertical mixing does not also lead to an upward flux of cold thermocline water[13].
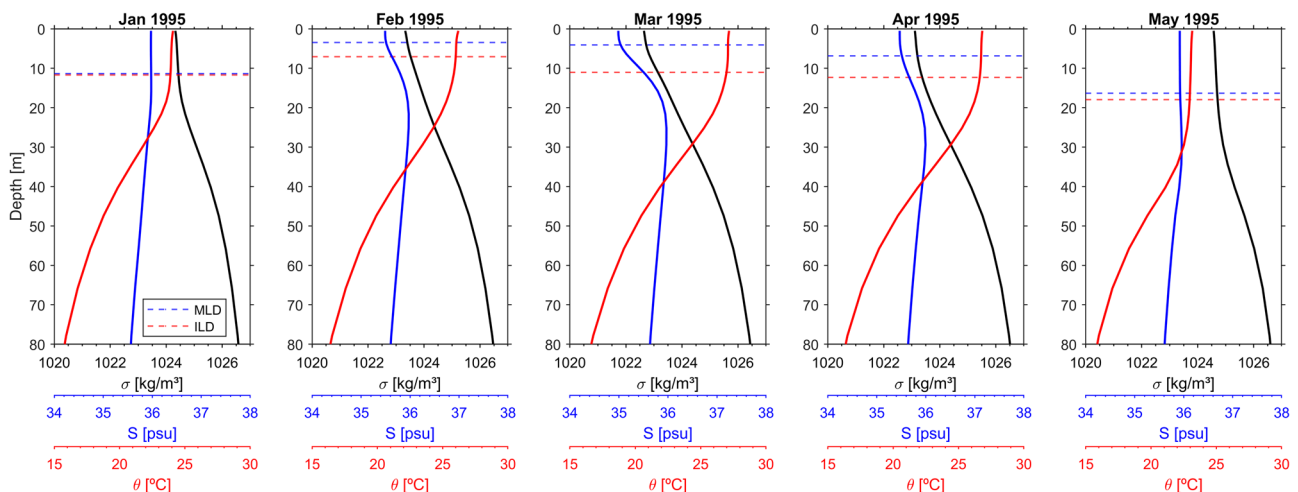
Fig. 7 | Vertical hydrographic structure in the Angola-Benguela Area. Monthly averaged vertical profiles of temperature (red), salinity (blue), and potential density (black) in the Angola Benguela Area (ABA; 10°S–20°S, 8°E–14°E) for January-May 1995 from the Global Ocean Eddy-resolving Reanalysis (GLORYS12). The mixed layer depth (MLD) and isothermal layer depth (ILD) for each month are indicated by horizontal blue and red lines, respectively. The barrier layer is defined as the region between these two layers.
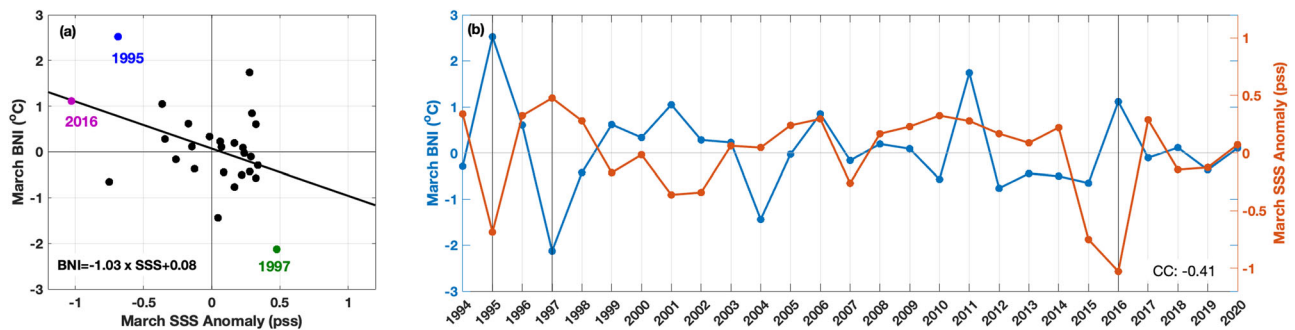
Fig. 8 | Low surface salinity in the Angola-Benguela Area is associated with stronger Benguela Niños. a Scatter diagram and linear regression fit between the BNI and ABA SSS in March when Benguela Niños and Niñas typically peak from the GLORYS12 reanalysis for the period 1993–2019. The years 1995 and 2016 (Benguela Niños following positive IOD events) and 1997 (Benguela Niña following a negative IOD event) are highlighted. **b** Time series of March BNI and SSS values with 1995, 1997, and 2016 indicated by vertical lines. The crosscorrelation (CC) of the two-time series shown in the lower right of panel (**b**) is −0.41, which is significantly nonzero with 90% confidence. The linear least squares regression fit equation is shown in (**a**).

In summary, as previously reported[13], the amplitude of the extraordinarily strong Benguela Niño in early 1995 (Fig. 1e) was boosted by anomalously high freshwater discharge from the Congo River that was advected southward in early 1995 (Fig. 6). The precise mechanism by which Congo River discharge amplified ABA warm SST anomalies was through the formation of thin, salt-stratified mixed layers overlying thick barrier layers that limited vertical mixing with colder temperatures in the thermocline (Fig. 7)[13]. The results of this study identify the ultimate cause of the anomalously high Congo River discharge as the 1994 Indian Ocean Dipole which peaked several months before the onset of the 1995 Benguela Niño (Fig. 1e). The IOD altered the atmospheric circulation to enhance moisture convergence and rainfall over the Congo River basin in late 1994 (Figs. 3, 4). Rain water runoff was then shunted by the Congo River into the eastern tropical Atlantic where it significantly lowered coastal salinity (Fig. 2), after which this fresh water mass was swept southward into the ABA. We emphasize that based on the evidence we have presented, the 1994 IOD helped to boost the amplitude of the 1995 Benguela Niño, but was not the ultimate cause for it. Warm anomalies were already developing in the ABA in January 1995 (Fig. 1e) before the major southward pulse of Congo River discharge in February 1995 (Fig. 6c,e).

Most previous wind-forced ocean model simulations of the 1995 Benguela Niño have tended to underestimate the amplitude of the event compared with observations[4–6,23]. In every case, these modeling studies failed to include the effect of Congo River discharge on barrier layer formation and the mixed layer heat balance. Our analysis suggests that including anomalous Congo River discharge in model simulations of Benguela Niños may help to reconcile this discrepancy. A previous idealized modeling study has suggested that Congo River discharge had little impact on SST in the region to the north of the ABA[24]. However, no similar modeling studies have been conducted in the ABA during the developing phase of Benguela Niños. Such studies would be a valuable contribution to further quantify the effects of barrier layer formation on Benguela Niño amplitudes in general and for the 1995 Benguela Niño in particular.

Indian Ocean Dipole effects on other Benguela Niños
The series of inter-basin events described in this paper appear to happen coincidentally, so one might not expect a systematic relationship between the IOD and Benguela Niños. There are, however, other Benguela Niños that appear to have been influenced by the IOD in a similar fashion, one of which occurred in 2016. This Benguela Niño was weaker than the 1995 event but as in 1995, enhanced freshwater input to the region from Congo River discharge helped to boost its amplitude[9]. This event was preceded in the boreal fall of 2015 by a moderate amplitude IOD event (Fig. 1c,d)[18] that altered the atmospheric circulation around Africa to converge moisture over the Congo River basin (Fig. 4d). While the various rainfall estimates (TAMSAT, GPCP, ERA5) are less in agreement on the overall magnitude of

the Congo River basin rainfall anomaly in late 2015 (cf. Figs. 4d and S2a, b), there were regions in the basin that experienced excess rainfall (Fig. S2e, f) and these regions likely contributed to the substantial increase in Congo River discharge in late 2015-early 2016 (Fig. S3c). Similar to what happened in early 1995, this river discharge and its southward advection along the coast of Angola and Namibia (Fig. S3) contributed to the formation of thin surface mixed layers, thick subsurface barrier layers and warmer coastal SSTs[9].

Previous research based on satellite observations has suggested that the salinity impacts of anomalous Congo River discharge on Benguela Niño development would only rarely occur and be difficult to observe[25]. However, recognizing the IOD's impact on Congo River discharge[17] facilitates identification of such events. Over the 40 year-long (1982–2021) DMI and Benguela Niño time series (Fig. 1), the events discussed in this article, namely 1994–95 and 2015–16, clearly stand out. However, there are other related events as well that appear in the record. For example, there was also a strong negative IOD event in late 1996 that was followed by a Benguela Niña in early 1997. We hypothesize that the mechanisms by which a positive IOD amplifies a Benguela Niño work equivalently but in an opposite sense for negative IOD events and Benguela Niñas like in 1996–97. For such events, reduced Congo River discharge would lead to elevated SSS and the absence of barrier layers in the ABA, facilitating enhanced vertical mixing and lower SSTs.

We also note that for the period 1993–2020, there is an inverse relationship between monthly SSS from the GLORYS12 reanalysis and the monthly BNI (Fig. 8) with a zero-lag crosscorrelation of −0.41 (significantly nonzero with 90% confidence). A regression fit to the data suggests that a 1 pss freshening of surface salinity would be associated with a 1 °C increase in Benguela Niño SST, while a 1 pss increase in salinity would be associated with anomalous surface cooling of 1 °C. The years 1995 and 2016 (Benguela Niños following positive IOD events) and 1997 (a Benguela Niña following a negative IOD event) stand out in the BNI and SSS scatterplot (Fig. 8). Correlation does not imply causality and there is ambiguity about cause and effect with BNI and SSS most highly correlated at zero lag. Rainfall does increase slightly in March 1995 associated with higher SSTs in the ABA as noted above (Fig. 5), but in general local rainfall is a small contributor to SSS variability during the development of Benguela Niños. The variations in mixed layer salt storage are more affected by horizontal advection and vertical exchanges (Fig. 6e). That suggests that low SSS is leading to higher SSTs more than the other way around. As evident from Fig. 7, advection of low salinity from the Congo discharge causes the mixed layer to shoal to only 5 m depth in February–March 1995. With such low heat capacity, the shallow mixed layer responds within a few days to heat exchanges across the air-sea interface. For example, a 20 W m^{-2} surface heat flux into a 5 m deep mixed layer would warm the mixed layer by about 1 °C in 10 days. Thus, a monthly time average does not resolve the detailed SST adjustment to

Article

surface heat flux trapped in such a shallow layer, which would explain the zero-lag correlation. Thus, we conclude that salinity changing the depth of the mixed layer so as to trap heat and raise SST is a more plausible first-order explanation for the SSS/BNI relationship than enhanced rainfall linked to unusually warm SST causing the salinity to drop.

It is interesting to note that associated with the easterly wind anomalies in the Indian Ocean linked to the development of the IOD in October 1994, there are low-level westerly wind anomalies evident in the equatorial Atlantic (Figs. 1b and 3). That is also true for the 2019 IOD[17]. These low-level westerly anomalies in the Atlantic are consistent with the atmospheric mass and moisture balance that require inflow to supply ascending air in the convective center over the Congo basin. Thus, it may be more than coincidence that the IOD is sometimes followed by a Benguela Niño event, in that the IOD-driven rainfall over the Congo may also result in low-level westerly wind anomalies along the equator in the Atlantic that contribute to the initiation of a subsequent Benguela Niño. Indeed, it has been noted that the IOD-related convection over Africa can weaken the Atlantic trade winds near the equator, thereby triggering Atlantic Niño events[26,27]. Weakened trade winds constitute remote forcing for Benguela Niños, which is why Atlantic Niños and Benguela Niños often occur together in the same year[4,6]. Our study has focused on Indian Ocean forcing of the Atlantic via a land bridge involving Congo River discharge. However, it is very plausible that IOD forcing of the Atlantic may occur simultaneously through both land and atmospheric bridges, a hypothesis that warrants further testing in a modeling framework that can incorporate both pathways.

Conclusions

Given the substantial environmental and economic impacts of Benguela Niños, there is tremendous societal value in developing skillful prediction models for these events. However, seasonal forecast skill for Atlantic SSTs in general and Benguela Niños in particular is limited to a few months at most[28–31]. This study suggests one potential new source of predictability for Benguela Niños, namely the IOD through both a land bridge involving the Congo River basin hydrology and possibly an atmospheric route involving convection over Africa. There is predictability built into the phase lags between IOD development, atmospheric circulation changes, Congo basin rainfall, Congo River discharge, and eastern tropical Atlantic SSS, with SSS lagging the DMI by 3–5 months (Figure S1). Thus, for a Benguela Niño that develops early in the calendar year following an IOD event, we might anticipate that its amplitude and impacts will be more pronounced than they would have otherwise been had there been no antecedent IOD. We can moreover gauge the likelihood for such an amplification by monitoring Congo River basin rainfall, river discharge, and eastern tropical Atlantic surface salinity anomalies. Ensuring that these processes are properly represented in Benguela Niño forecast models should be a priority.

Finally, there is a diversity of IOD events in terms of their amplitude, spatial structure, and temporal evolution[32]. It has been suggested from climate model simulations under high greenhouse gas emission scenarios that the frequency of extreme IOD events, like the 1994 event which boosted the amplitude of the 1995 Benguela Niño, will increase by almost a factor of three over the course of the twenty-first century[33]. This represents an increase from one extreme IOD event every 17 years during the twentieth century to one extreme event every 6 years by the end of the 21st century. If this increase in frequency is realized, it is likely that future IOD events will exert much more influence than today on Benguela Niño development through both the land bridge which has been the focus of this study, and possibly also through an atmospheric bridge as suggested in refs. 26,27.

Data and methods
Data sources and indices
We used monthly mean SST data from the high-resolution NOAA Optimum Interpolation SST (OISST) data set, consisting of blended satellite and in-situ measurements from 1981 to present, with spatial resolution of 0.25°[34,35].

We define the Dipole Mode Index (DMI), a measure of IOD strength, as the SST anomaly difference between the eastern (90°E–110°E, 10°S–0°N) and western (50°E–70°E, 10°S–10°N) equatorial Indian ocean. We define the Benguela Niño Index (BNI) as the average of SST anomalies in the ABA (10°S–20°S, 8°E–14°E). Anomalies are based on a 30-year climatology for 1991–2020. A long-term linear trend has been removed from the BNI time series.

IOD events occur with both positive and negative polarity. Positive events like 1995 (DMI > 1 standard deviation) are associated with unusually cold SSTs in the eastern Indian Ocean, unusually warm SSTs in the western Indian Ocean, and anomalous easterly surface winds (Fig. 1b). Negative events (DMI < −1 standard deviation) are associated with anomalies of opposite sign. Similarly, there is a cold counterpart to Benguela Niños (BNI > 1 standard deviation), referred to as Benguela Niñas (BNI < −1 standard deviation), that occur when SSTs in the ABA are significantly colder than climatology.

Congo River discharge is based on daily data measured at Kinshasa-Brazzaville station 500 km upstream from the river mouth, for January 1954 to February 2020, available from the Global Runoff Data Centre. We use two different monthly rainfall data sets, one of which is from the Global Precipitation Climatology Project (GPCP) at 0.5° spatial resolution from 1979 to 2021[36]. The second is the Tropical Applications of Meteorology using SATellite (TAMSAT) data, available from the University of Reading for 1983–2020, which are based on ground-based observations at 0.0375° spatial resolution from land areas only. Comparison of these two data sets[17] indicates that they provide complementary and consistent views of rainfall variability in the region.

Monthly temperature, salinity, ocean currents, sea level, and mixed layer depth are taken from the Global Ocean Eddy-resolving Reanalysis (GLORYS12)[37], with 1/12° horizontal resolution and 50 vertical levels, of which 22 are in the upper 100 m. The reanalysis is based on the Nucleus for European Modelling of the Ocean (NEMO) with atmospheric forcing by the European Centre for Medium-Range Weather Forecasts (ECMWF) Interim Reanalysis (ERA-Interim) and the ECMWF Reanalysis v5 (ERA5) in recent years. Assimilated observations include Reynolds 0.25° AVHRR-only SST, delayed mode sea level anomaly from all altimetric satellites, in situ temperature/salinity profiles from Copernicus Marine CORAv4.1 database, and IFREMER/CERSAT sea ice concentration. GLORYS12 only incorporates climatological monthly mean river runoff but the effects of interannual variations in runoff are included though data assimilation in the model. The reanalysis is available from 1993 onward and we use output for the period 1993-2020.

Temperature and salinity data in upper 200 m of the reanalysis product in the southeastern tropical Atlantic were previously validated against independent in-situ measurements from the Nansen Programme[13], which comprises more than 8000 Conductivity-Depth-Temperature (CTD) profiles taken off the Angola and Namibia coasts from 1994–2014[38]. Although the GLORYS12 reanalysis is forced with climatological river runoff, validation against the CTD profiles showed correlation and root-mean square deviation of 0.68 (0.96) and 0.55 pss (1.3 °C), respectively, for the salinity (temperature) values in the coastal zone[13].

Monthly specific humidity, atmospheric winds at several pressure levels ranging from 1000–1 hPa, surface rate of evaporation, surface rate of precipitation, and the vertically integrated atmospheric moisture budget terms at 0.25° spatial resolution during 1987–2021 are obtained from the ERA5[39,40].

Ocean mixed layer salt balance
We use a mixed-layer salt balance equation in the ABA to relate the change in mixed-layer salinity to local surface forcing and horizontal advection. This equation can be written as

$$\frac{\partial S}{\partial t} = -\mathbf{u} \cdot \nabla \mathbf{S} + \mathrm{FW_{forc}} + \mathrm{Res.} \qquad (1)$$

where $\frac{\partial S}{\partial t}$ is the time rate of mixed layer salinity (S). Horizontal advection is the first term on the right side of the equation, with $\mathbf{u}$ as the horizontal vector velocity in the mixed layer and ∇S is the two-dimensional horizontal salinity gradient. The local freshwater forcing term is computed using

$$\mathrm{FW_{forc}} = \frac{\mathrm{So}}{\mathrm{h}}(\mathrm{E} - \mathrm{P}) \qquad (2)$$

where E is the rate of evaporation (in m day^{-1}), P is the rate of precipitation (in m day^{-1}), S_o is the surface salinity (in pss) and h is the mixed layer depth (in m). The residual term (Res) includes terms that cannot be explicitly computed (such as vertical advection, entrainment, and diffusion) and any computational errors.

Atmospheric moisture budget

We use ERA5 monthly evaporation and precipitation, monthly sea surface salinity, horizontal velocities, and mixed layer depth from the GLORYS12 reanalysis to estimate terms in (1). $E - P$ estimates in this calculation are essentially the same when the ERA5 precipitation is replaced by GPCP precipitation.

The atmospheric moisture budget equation can be written as:

$$\mathrm{E} - \mathrm{P} = \frac{1}{g}\nabla.\int_{\mathrm{pt}}^{\mathrm{ps}} \mathrm{qVdp} + \frac{1}{g}\frac{\partial}{\partial t}\int_{\mathrm{pt}}^{\mathrm{ps}} \mathrm{qdp} \qquad (3)$$

where P and E are rates of precipitation and evaporation (in kg m^{-2} s^{-1}), g is acceleration due to gravity (m^2 s^{-1}), q is specific humidity (kg/kg), v is the horizontal wind vector (m/s), ps is surface pressure 1000 hPa and pt is pressure at the uppermost level of the atmosphere, chosen to be 100 hPa. The first and second terms on the right-hand side of the equation denote the divergence field of moisture flux and the moisture tendency, respectively. In order to determine the relative contribution of dynamic and thermo-dynamic processes to the moisture divergence term, we decompose the wind and specific humidity as $V = \bar{V} + V'$ and $q = \bar{q} + q'$, where $\bar{V}, \bar{q}$ are the climatological means over the period 1987–2020 and V', q' are the deviations from the 34-year climatology[41,42]. Moisture divergence can then be written as the sum of dynamic (DYN), thermodynamic (TD) and transient eddy (TE) components estimated using:

$$\mathrm{DYN} = \frac{1}{g}\nabla.\int_{\mathrm{pt}}^{\mathrm{ps}} \bar{\mathrm{q}}\mathrm{V'dp} \qquad (4)$$

$$\mathrm{TD} = \frac{1}{g}\nabla.\int_{\mathrm{pt}}^{\mathrm{ps}} \mathrm{q'}\bar{\mathrm{V}}\mathrm{dp} \qquad (5)$$

$$\mathrm{TE} = \frac{1}{g}\nabla.\int_{\mathrm{pt}}^{\mathrm{ps}} \mathrm{q'V'dp} \qquad (6)$$

All units in kg m^{-2} s^{-1}. We find that the TE component is negligible compared to the DYN and TD components of moisture divergence as the deviations of q and V from the climatology are quite small. Thus, we do not consider it further in our analysis.

Reporting Summary

Further information on research design is available in the Nature Portfolio Reporting Summary linked to this article.

Data availability

All the datasets are freely available in the public domain. OISST data are available at National Centers for Environmental Information (www.ncei. noaa.gov). Daily in situ measurements of river discharge measured at Kinshasa-Brazzaville station were obtained from the Global Runoff Data Centre (https://www.bafg.de/GRDC/EN/Home/homepage_node.html). TAMSAT data are available at https://www.tamsat.org.uk/ and GPCP data

are available at (https://data.nasa.gov/dataset/GPCPPrecipitation-Level-3-Monthly-0-5-Degree-V3-2/2kyxn57r/data). The GLORYS12 reanalysis is distributed by the EU Copernicus Marine Service Information (http://marine.copernicus.eu/) and monthly ERA5 data can be accessed at https://www.ecmwf.int/en/forecasts/dataset/ecmwf-reanalysis-v5.

Code availability

We use basic statistics packages and plotting methods in MATLAB and Python for the analysis. We do not use any specific code for data processing. The codes used in this study are available upon request to the second author S.J.

References

1. Boyer, D. C., Boyer, H. J., Fossen, I. & Kreiner, A. Changes in abundance of the northern Benguela sardine stock during the decade 1990–2000, with comments on the relative importance of fishing and the environment. *Afr. J. Mar. Sci.* **23**, 67–84 (2001).
2. Rouault, M., Florenchie, P., Fauchereau, N. & Reason, C. J. C. South East tropical Atlantic warm events and southern African rainfall. *Geophys. Res. Lett*. **30**, 8009 https://doi.org/10.1029/2002GL014840 (2003).
3. Lübbecke, J. F. et al. Equatorial Atlantic variability—modes, mechanisms, and global teleconnections. *WIREs Clim. Change* **9**, e527 (2018).
4. Illig, S., Bachèlery, M.-L. & Lübbecke, J. F. Why do Benguela Niños lead Atlantic Niños? *J. Geophys. Res.* **125**, e2019JC016003 (2020).
5. Florenchie, P. et al. Evolution of interannual warm and cold events in the southeast Atlantic Ocean. *J. Clim.* **17**, 2318–2334 (2004).
6. Lübbecke, J. F., Böning, C. W., Keenlyside, N. S. & Xie, S.-P. On the connection between Benguela and equatorial Atlantic Niños and the role of the South Atlantic anticyclone. *J. Geophys. Res.* **115**, C09015 (2010).
7. Imbol Koungue, R. A., Illig, S. & Rouault, M. Role of interannual Kelvin wave propagations in the equatorial Atlantic on the Angola Benguela Current system. *J. Geophys. Res.* **122**, 4685–4703 (2017).
8. Richter, I. et al. On the triggering of Benguela Niños: remote equatorial versus local influences. *Geophys. Res. Lett.* **37**, L20604 (2010).
9. Lübbecke, J. F. et al. Causes and evolution of the southeastern tropical Atlantic warm event in early 2016. *Clim. Dyn.* **53**, 261–274 (2019).
10. Imbol Koungue, R. A. & Brandt, P. Impact of intraseasonal waves on Angolan warm and cold events. *J. Geophys. Res.* **126**, e2020JC017088 (2021).
11. Imbol Koungue, R. A. et al. The 2019 Benguela Niño. *Front. Mar. Sci.* **8**, 800103 (2021).
12. Gammelsrød, T., Bartholomae, C. H., Boyer, D. C., Filipe, V. L. L. & O'Toole, M. J. Intrusion of warm surface water along the Angolan-Namibian coast in February–March 1995: the 1995 Benguela Niño. *So. Afr. J. Mar. Sci.* **19**, 41–56 (1998).
13. Aroucha, L. C., Lübbecke, J. F., Korner, M., Imbol Koungue, R. A. & Awo, F. M. The influence of freshwater input on the evolution of the 1995 Benguela Niño. *J. Geophys. Res.* **129**, e2023JC020241 (2024).
14. Saji, N. H., Goswami, B. N., Vinayachandran, P. N. & Yamagata, T. A dipole mode in the tropical Indian Ocean. *Nature* **401**, 360–363 (1999).
15. Webster, P. J., Moore, A. M., Loschnigg, J. P. & Leben, R. R. Coupled ocean–atmosphere dynamics in the Indian Ocean during 1997–98. *Nature* **401**, 356–360 (1999).
16. Moihamette, F., Pokam, W. M., Diallo, I. & Washington, R. Extreme Indian Ocean dipole and rainfall variability over Central Africa. *Int. J. Climatol.* **42**, 5255–5272 (2022).

17. Jarugula, S. & McPhaden, M. J. Indian Ocean Dipole affects eastern tropical Atlantic salinity through Congo River Basin hydrology. *Nat. Comm. Earth Environ.* **4**, 366 (2023).

18. Utari, P. A., Khakim, M. Y. H., Setiabudidaya, D. & Iskandar, I. Dynamics of 2015 positive Indian Ocean Dipole. *J. South. Hemisph. Earth Sys. Sci.* **69**, 75–83 (2019).

19. Alsdorf, D. et al. Opportunities for hydrologic research in the Congo Basin. *Rev. Geophys.* **54**, 378–409 (2016).

20. Fennel, W., Junker, T., Schmidt, M. & Mohrholz, V. Response of the Benguela upwelling systems to spatial variations in the wind stress. *Cont. Shelf Res.* **45**, 65–77 (2012).

21. Palma, E. D. & Matano, R. P. An idealized study of near equatorial river plumes. *J. Geophys. Res.* **122**, 3599–3620 (2017).

22. Vic, C., Berger, H., Tréguier, A. & Couvelard, X. Dynamics of an equatorial river plume: theory and numerical experiments applied to the Congo plume case. *J. Phys. Oceanogr.* **44**, 980–994 (2014).

23. Imbol Koungue, R. A., Rouault, M., Illig, S., Brandt, P. & Jouanno, J. Benguela Niños and Benguela Niñas in forced ocean simulation from 1958 to 2015. *J. Geophys. Res.* **124**, 5923–5951 (2019).

24. White, R. H. & Toumi, R. River flow and ocean temperatures: The Congo River. *J. Geophys. Res. Oceans* **119**, 2501–2517 (2014).

25. Martins, M. S. & Stammer, D. Interannual Variability of the Congo River Plume-Induced Sea Surface Salinity. *Remote Sens.* **14**, 1013 (2022).

26. Zhang, L. & Han, W. Indian Ocean Dipole leads to Atlantic Niño. *Nat. Commun.* **12**, 5952 (2021).

27. Fan, L. & Meng, X. The Asymmetric predictive power of Indian Ocean Dipole for subsequent year's ENSO: Role of Atlantic Ocean as an intermediary. *Geophys. Res. Lett.* **50**, e2023GL105525 (2023).

28. Li, X., Bordbar, M. H., Latif, M., Park, W. & Harlaß, J. Monthly to seasonal prediction of tropical Atlantic sea surface temperature with statistical models constructed from observations and data from the Kiel Climate model. *Clim. Dyn.* **54**, 1829–1850 (2020).

29. Li, X., Tan, W., Hu, Z.-Z. & Johnson, N. C. Evolution and prediction of two extremely strong Atlantic Niños in 2019–2021: impact of Benguela Warming. *Geophys. Res. Lett.* **50**, e2023GL104215 (2023).

30. Oettli, P., Yuan, C. & Richter, I. The other coastal Niño/Niña—the Benguela, California, and Dakar Niños/Niñas. in *Tropical and Extratropical Air-Sea Interactions* (ed. Behera, S. K.) 237–266. https://doi.org/10.1016/B978-0-12-818156-0.00010-1.466 (Elsevier, 2021).

31. Wang, R., Chen, L., Li, T. & Luo, J.-J. Atlantic Niño/Niña prediction skills in NMME models. *Atmosphere* **12**, 803 (2021).

32. Cai, W. et al. Opposite response of strong and moderate positive Indian Ocean Dipole to global warming. *Nat. Clim. Chang.* **11**, 27–32 (2021).

33. Cai, W. et al. Increased frequency of extreme Indian Ocean Dipole events due to greenhouse warming. *Nature* **510**, 254–258 (2014).

34. Huang, B. et al. Improvements of the daily optimum interpolation sea surface temperature (DOISST) version 2.1. *J. Clim.* **34**, 2923–2939 (2021).

35. Reynolds, R. W. et al. Daily high-resolution-blended analyses for sea surface temperature. *J. Clim.* **20**, 5473–5496 (2007).

36. Adler, R. F. et al. The version-2 global precipitation climatology project (GPCP) monthly precipitation analysis (1979–present). *J. Hydrometeorol.* **4**, 1147–1167 (2003).

37. Lellouche, J.-M. et al. The copernicus global 1/12 oceanic and sea ice GLORYS12 reanalysis. *Front. Earth Sci.* **9**, 1–27 (2021).

38. Tchipalanga, P., Ostrowski, M., & Dengler, M. Physical oceanography on the Angolan continental shelf and Cabinda. *PANGAEA.* https://doi.org/10.1594/PANGAEA.886492 (2018).

39. Hersbach, H., et al ERA5 monthly averaged data on pressure levels from 1940 to present. *Copernicus Climate Change Service (C3S) Climate Data Store (CDS).* https://doi.org/10.24381/cds.6860a573 (2023).

40. Mayer, J., Mayer, M., Haimberger, L., Mass-consistent atmospheric energy and moisture budget monthly data from 1979 to present derived from ERA5 reanalysis. *Copernicus Climate Change Service (C3S) Climate Data Store (CDS).* https://doi.org/10.24381/cds.c2451f6b (2021).

41. Seager, R., Naik, N. & Vecchi, G. A. Thermodynamic and dynamic mechanisms for large-scale changes in the hydrological cycle in response to global warming. *J. Clim.* **23**, 4651–4668 (2010).

42. Wang, Z., Duan, A., Yang, S. & Ullah, K. Atmospheric moisture budget and its regulation on the variability of summer precipitation over the Tibetan Plateau. *J. Geophys. Res. Atmos.* **122**, 614–630 (2017).

Author contributions
M.J.M. conceived of the study and wrote the first draft. S.J. and L.C.A. contributed analyses and graphics. All authors (M.J.M, S.J., L.C.A., and J.F.L.) contributed to the interpretation of the results and to writing and editing the final manuscript.

Competing interests
The authors declare no competing interests.

Additional information
Supplementary information The online version contains supplementary material available at https://doi.org/10.1038/s43247-024-01955-x.

Correspondence and requests for materials should be addressed to Michael J. McPhaden.

Peer review information *Communications Earth & Environment* thanks Lei Fan and the other, anonymous, reviewer(s) for their contribution to the peer review of this work. Primary Handling Editors: José Luis Iriarte Machuca and Alireza Bahadori. A peer review file is available.

Reprints and permissions information is available at http://www.nature.com/reprints

Publisher's note Springer Nature remains neutral with regard to jurisdictional claims in published maps and institutional affiliations.